Protein Farnesyltransferase Isoprenoid Substrate Discrimination Is Dependent on Isoprene Double Bonds and Branched Methyl Groups†

Eugenio Micali,[||,‡] Kareem A. H. Chehade,[||,‡] Richard J. Isaacs,[‡,§] Douglas A. Andres,[‡,§] and H. Peter Spielmann*[,‡,§,⊥]

Department of Molecular and Cellular Biochemistry, Department of Chemistry, and Kentucky Center for Structural Biology, University of Kentucky, Lexington, Kentucky 40536-0084

Received June 1, 2001; Revised Manuscript Received August 20, 2001

ABSTRACT: Farnesylation is a posttranslational lipid modification in which a 15-carbon farnesyl isoprenoid is linked via a thioether bond to specific cysteine residues of proteins in a reaction catalyzed by protein farnesyltransferase (FTase). We synthesized the benzyloxyisoprenyl pyrophosphate (BnPP) series of transferable farnesyl pyrophosphate (FPP) analogues (**1a**−**e**) to test the length dependence of the isoprenoid substrate on the FTase-catalyzed transfer of lipid to protein substrate. Kinetic analyses show that pyrophosphates **1a**−**e** and geranyl pyrophosphate (GPP) transfer with a lower efficiency than FPP whereas geranylgeranyl pyrophosphate (GGPP) does not transfer at all. While a correlation was found between K_m and analogue hydrophobicity and length, there was no correlation between k_{cat} and these properties. Potential binding geometries of FPP, GPP, GGPP, and analogues **1a**−**e** were examined by modeling the molecules into the active site of the FTase crystal structure. We found that analogue **1d** displaces approximately the same volume of the active site as does FPP, whereas GPP and analogues **1a**−**c** occupy lesser volumes and **1e** occupies a slightly larger volume. Modeling also indicated that GGPP adopts a different conformation than the farnesyl chain of FPP, partially occluding the space occupied by the Ca_1a_2X peptide in the ternary X-ray crystal structure. Within the confines of the FTase pocket, the double bonds and branched methyl groups of the geranylgeranyl chain significantly restrict the number of possible conformations relative to the more flexible lipid chain of analogues **1a**−**e**. The modeling results also provide a molecular explanation for the observation that an aromatic ring is a good isostere for the terminal isoprene of FPP.

Protein farnesyltransferase (FTase)[1] catalyzes the transfer of a 15-carbon farnesyl isoprenoid from farnesyl pyrophosphate (FPP) to a conserved cysteine of its protein substrate, forming a thioether bond (*1*, *2*). The reactive cysteine is located in the C-terminal Ca_1a_2X motif in which C is the modified cysteine, a_1 and a_2 are often an aliphatic residue, and X is Ser, Met, Ala, or Gln. Farnesylation is the first and obligatory step in an ordered series of posttranslational modifications which mediate membrane localization and possibly protein−protein interactions for a variety of proteins involved in cellular regulatory events (*3*−*5*). The farnesylation of Ras proteins has received much attention since the discovery that oncogenic forms of these proteins require modification in order to transform cells (*6*, *7*). As a result, FTase has emerged as a major target for the development of anti-cancer therapeutics and is the subject of numerous structural and structure−function analyses as part of a widespread program to develop selective inhibitors (FTIs) (*8*−*12*). Several potent inhibitors of FTase have been identified which prevent in vivo farnesylation.

Analogues of FPP that are alternative transferable substrates for FTase have been utilized to study farnesylation and subsequent downstream processing events (*13*−*18*). Simple FPP analogues stripped of most isoprenoid features such as methyl groups and unsaturation to more resemble simple fatty acids are transferred to Ras by FTase and allow Ras to function in a *Xenopus* signal transduction model system (*15*). The 3-methyl group has been modified in attempts to make mechanism-based inhibitors and probes for the mechanism of transfer (*13*, *14*, *17*, *19*, *20*). Some of these molecules are transferable by FTase to protein substrates while others serve as FTIs.

However, there is limited information available on the structural features of the lipid that allow transfer by FTase. Appropriate transfer of an FPP analogue to a peptide substrate by FTase is dependent on the length of the lipid. The shorter and less hydrophobic GPP is transferred by

† This work was supported in part by the National Institutes of Health (Grant EY11231 to D.A.A.), the National Science Foundation (Grant MCB-9808633 to H.P.S.), the Kentucky Medical Center Research Fund (Grant 831 to H.P.S.), and the Kentucky-NSF EPSCoR Program (Grant EPS-9452895 to H.P.S.).

* To whom correspondence should be addressed. Telephone: 859-257-4790. Fax: 859-257-8940. E-mail: hps@uky.edu.

‡ Department of Molecular and Cellular Biochemistry.

§ Kentucky Center for Structural Biology.

|| Authors contributed equally to this work.

⊥ Department of Chemistry.

[1] Abbreviations: FTase, protein farnesyltransferase; FPP, farnesyl pyrophosphate; GPP, geranyl pyrophosphate; GGPP, geranylgeranyl pyrophosphate; FTI, farnesyl transferase inhibitor; AGPP, 8-anilinogeranyl pyrophosphate; BnPP, benzyloxyisoprenyl pyrophosphate; NMR, nuclear magnetic resonance; HPLC, high-performance liquid chromatography; AMBER, assisted model building and energy refinement; rms, root-mean-square.

10.1021/bi011133f CCC: $20.00
Published on Web 09/14/2001

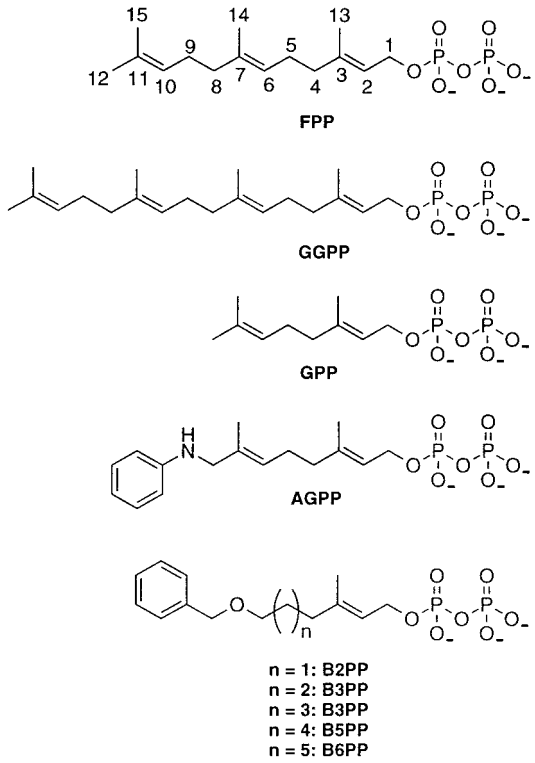

FIGURE 1: Structures of farnesyl pyrophosphate (FPP), geranylgeranyl pyrophosphate (GGPP), geranyl pyrophosphate (GPP), and transferable FPP analogues 8-anilinogeranyl pyrophosphate (AGPP), B2PP, B3PP, B4PP, B5PP, and B6PP.

FTase to H-Ras; however, the 20-carbon isoprenoid geranylgeranyl pyrophosphate (GGPP) is not (*15*, *21*, *22*). Analysis of the FTase crystal structures suggests that the FPP binding pocket on the enzyme is too shallow to allow the longer GGPP to bind in a productive conformation (*23*−*26*). The depth of the hydrophobic FPP binding pocket in FTase is postulated to function as a molecular ruler that discriminates between the natural substrate FPP and GGPP. The ruler measures the span from the aromatic residues at the bottom of the hydrophobic cavity to the positive cleft at the top rim of the α−α barrel where the pyrophosphate binds and the catalytic zinc ion is found. In this model, geranylgeranyl transfer by FTase is prevented by forcing the C_1 position of the bound GGPP to protrude beyond the catalytic zinc ion. This hypothesis implies that productive substrate binding is dependent on the isoprenoid conformation. However, substrate discrimination is dependent upon additional factors since the much shorter GPP is also transferred by FTase to peptide substrate with much lower efficiency.

The structure of the ω-terminal group of FPP analogues (Figure 1) has been found to profoundly influence the ability of FTase to transfer lipid analogues to target proteins (*15*, *27*−*36*). Incorporation of photoreactive functionality and heteroatoms on the ω-terminus of FPP analogues generated FTIs (*27*−*36*). However, substitution of the terminal isoprene with an aniline group resulted in a transferable analogue (*18*). The FPP analogue 8-anilinogeranyl pyrophosphate (AGPP) is transferred to Ras by FTase with the same kinetics as FPP. This result suggests that an aniline group is an isostere for the terminal isoprene moiety of FPP with respect to binding to FTase and transfer to protein substrate.

Much less is known about the structural requirements for the β-isoprene unit of FPP on the FTase-catalyzed transfer of lipid to target protein. FPP analogues where the β- and ω-isoprene double bonds (6,7 and 10,11) are saturated and where both the β- and ω-isoprene double bonds are saturated and the 7- and 11-methyl groups were missing are transferable by FTase (*15*). However, it is not clear what effect these modifications have on the transfer efficiency of the analogues.

We report the synthesis and biochemical characterization of the benzyloxyisoprenyl pyrophosphate (BnPP) series of FPP analogues (**1a**−**e**). These molecules were designed to test the effect modification of the β-isoprene to an alkyl-ether chain of variable length and of replacement of the ω-terminal isoprene unit of the farnesyl group with a benzyloxy functionality had on the FTase-catalyzed transfer to substrate. All of the analogues are transferred to the dansyl-GCVLS peptide substrate by FTase with a lower efficiency than FPP. Comparison of the analogue structures and kinetics of analogue transfer with those of FPP, GPP, and GGPP reveals that the conformational restrictions imposed by the methyl branching and unsaturation of the β-isoprene may play an important role in substrate discrimination by FTase. We also find that the benzyl group is an acceptable isostere for the ω-isoprene of FPP and that incorporation of an ether linkage in the chain significantly reduces the affinity of the analogue pyrophosphate for FTase. This information, along with models of the substrate binding modes, will be useful in the design and synthesis of additional substrate analogues and mechanism-based FTase inhibitors.

EXPERIMENTAL PROCEDURES

General Chemical Procedures. All reactions were conducted under dry argon and stirred magnetically except as noted. Reaction temperatures refer to the external bath temperatures except as noted. Analytical TLC was performed on precoated (0.25 mm) silica gel 60F-254 (Merck) plates. Visualization was achieved either by UV irradiation or by anisaldehyde−sulfuric acid spray followed by heating. Flash chromatography was performed on Merck silica gel 60 (230−400 mesh ASTM). All chromatography solvents were purchased from VWR (EM Science-Omnisolv high purity grade) and used as received. Anhydrous acetonitrile, pyridine, and DME were purchased from Aldrich; anhydrous THF was purchased from Fluka; all other reagents were purchased either from Aldrich or from Pfaltz and Bauer, unless otherwise noted. NMR spectra were obtained in $CDCl_3$ (unless otherwise noted) at 200 MHz or at 400 MHz. Chemical shifts for the following deuterated solvents are reported in ppm downfield using the indicated reference peaks: $CDCl_3$ ($CDCl_3$ internal peak, 7.27 ppm for ^1H, 77.4 ppm for ^{13}C), D_2O (TSP, 0 ppm for ^1H and ^{13}C; H_3PO_4 as an external reference, 0 ppm for ^{31}P). Mass spectra were obtained from the University of Kentucky Mass Spectra Facility. HPLC pyrophosphate purifications were carried out by monitoring at 214 nm using a preparative Vydac C_{18} (218TP1010) column, and eluted under the following gradient at a flow rate of 4 mL/min: 0−6 min, 100% A; 6−18 min, 5% A; 18−19 min, 5% A; 19−28 min, 100% A; 28−35 min, 100% A. Solvents: A = 25 mM NH_4HCO_3; B = CH_3CN. HPLC analysis of fluorescence product studies was carried out using a Hewlett-Packard Series 1100 system equipped with a UV (monitoring at 254 nm) and fluorescence detector (340 nm excitation, 505 nm emission).

*General Procedure for Monobenzylated α,ω-Alkyldiols (**3a**−**e**) (37).* Solid potassium hydroxide (85%, 132.0 g, 2.0 mol) was added to the glycol (5.0 mol) and stirred until dissolution. The temperature was then increased to 90 °C (internal temperature), and benzyl chloride (180.2 g, 2.0 mol) was added while keeping the temperature of the reaction mixture at 90 °C (internal temperature). The temperature was then raised to 130 °C (internal temperature) and kept at this point for 2 h longer. The reaction mixture was then cooled, diluted with water, and extracted with Et_2O. The extract was washed with water, dried ($MgSO_4$), filtered, and evaporated. The residue was purified by distillation under reduced pressure to afford the benzyloxy ether as a colorless oil.

*(A) 2-Benzyloxyethanol (**3a**):* bp 90−95 °C/0.7 mmHg (62%). ^{1}H NMR δ 7.32−7.40 (m, 5H), 4.58 (s, 2H), 3.77 (t, 2H, J = 5.0 Hz), 3.61 (t, 2H, J = 5.0 Hz), 2.47 (s, 1H); ^{13}C NMR δ 138.34, 128.85, 128.19, 73.58, 71.72, 62.13.

*(B) 3-Benzyloxy-1-propanol (**3b**):* bp 95−100 °C/0.7 mmHg (67%). ^{1}H NMR δ 7.34−7.39 (m, 5H), 4.55 (s, 2H), 3.79 (t, 2H, J = 5.6 Hz), 3.68 (t, 2H, J = 6.0 Hz), 2.63 (s, 1H), 1.84−1.93 (m, 2H); ^{13}C NMR δ 138.47, 128.82, 128.07, 128.02, 73.53, 69.47, 61.88, 32.38.

*(C) 4-Benzyloxy-1-butanol (**3c**):* bp 102−105 °C/0.7 mmHg (67%). ^{1}H NMR δ 7.30−7.38 (m, 5H), 4.53 (s, 2H), 3.62 (t, 2H, J = 6.0 Hz), 3.52 (t, 2H, J = 5.8 Hz), 2.90 (s, 1H), 1.64−1.73 (m, 4H); ^{13}C NMR δ 138.53, 128.80, 128.08, 73.33, 70.63, 62.85, 30.26, 26.87.

*(D) 5-Benzyloxy-1-pentanol (**3d**):* bp 105−110 °C/0.7 mmHg (71%). ^{1}H NMR δ 7.31−7.37 (m, 5H), 4.50 (s, 2H), 3.61 (t, 2H, J = 6.2 Hz), 3.48 (t, 2H, J = 6.4 Hz), 2.10 (s, 1H), 1.40−1.68 (m, 6H); ^{13}C NMR δ 138.92, 128.76, 128.05, 127.94, 73.25, 70.62, 63.01, 32.72, 29.70, 22.68.

*(E) 6-Benzyloxy-1-hexanol (**3e**) (38−43):* bp 115−120 °C/0.7 mmHg (63%). ^{1}H NMR δ 7.26−7.35 (m, 5H), 4.50 (s, 2H), 3.62 (t, 2H, J = 6.6 Hz), 3.47 (t, 2H, J = 6.2 Hz), 1.36−1.65 (m, 9H); ^{13}C NMR δ 138.92, 128.70, 128.00, 127.86, 73.24, 70.68, 63.18, 33.05, 33.01, 26.37, 25.95.

*General Procedure for Methanesulfonates **4a**−**e**.* To a cooled (0 °C) solution of the benzyloxy alcohol **3a**−**e** (150.0 mmol) in anhydrous pyridine (60 mL) was added methanesulfonyl chloride (165.0 mmol, 18.9 g). The reaction mixture was stirred for 3 h at 0 °C, then diluted with water, and extracted with Et_2O. The organic solution was washed (10% HCl, then water, then 10% $NaHCO_3$, then water), dried ($MgSO_4$), filtered, and evaporated to obtain a colorless oil that was used in the next step without further purification.

*(A) 2-Benzyloxyethanol methanesulfonate (**4a**) (44−47):* 90%. ^{1}H NMR δ 7.34−7.37 (m, 5H), 4.59 (s, 2H), 4.40 (t, 2H, J = 4.8 Hz), 3.75 (t, 2H, J = 4.8 Hz), 3.03 (s, 3H); ^{13}C NMR δ 137.79, 128.90, 128.34, 128.16, 73.63, 69.49, 68.11, 37.92.

*(B) 3-Benzyloxy-1-propanol methanesulfonate (**4b**) (45, 48, 49):* 88%. ^{1}H NMR δ 7.35−7.39 (m, 5H), 4.54 (s, 2H), 4.39 (t, 2H, J = 6.2 Hz), 3.62 (t, 2H, J = 6.0 Hz), 2.98 (s, 3H), 2.01−2.11 (m, 2H); ^{13}C NMR δ 138.39, 128.78, 128.06, 73.37, 67.63, 65.76, 37.30, 29.72.

*(C) 4-Benzyloxy-1-butanol methanesulfonate (**4c**) (48, 50, 51):* 94%. ^{1}H NMR δ 7.25−7.33 (m, 5H), 4.49 (s, 2H), 4.24 (t, 2H, J = 6.2 Hz), 3.51 (t, 2H, J = 6.0 Hz), 2.95 (s, 3H), 1.68−1.91 (m, 4H); ^{13}C NMR δ 138.75, 128.81, 128.04, 73.36, 70.39, 69.74, 37.67, 26.64, 26.11.

*(D) 5-Benzyloxy-1-pentanol methanesulfonate (**4d**) (52):* 90%. ^{1}H NMR δ 7.35−7.39 (m, 5H), 4.53 (s, 2H), 4.26 (t, 2H, J = 6.6 Hz), 3.52 (t, 2H, J = 6.0 Hz), 3.02 (s, 3H), 1.50−1.90 (m, 6H); ^{13}C NMR δ 138.89, 128.79, 128.05, 127.98, 73.30, 70.32, 70.21, 37.64, 29.41, 29.22, 22.56.

*(E) 6-Benzyloxy-1-hexanol methanesulfonate (**4e**) (39, 53):* 84%. ^{1}H NMR δ 7.27−7.35 (m, 5H), 4.50 (s, 2H), 4.22 (t, 2H, J = 6.6 Hz), 3.47 (t, 2H, J = 6.2 Hz), 2.99 (s, 3H), 1.40−1.80 (m, 8H); ^{13}C NMR δ 138.88, 128.71, 127.98, 127.88, 73.27, 70.46, 70.42, 37.70, 29.91, 29.43, 26.06, 25.65.

*General Procedure for Iodides **5a**−**e**.* To a solution of NaI (58.5 g, 390.0 mmol) in acetone (250 mL) was added at room temperature a solution of the methanesulfonate **4a**−**e** (130.0 mmol) in acetone (50 mL). After the mixture was stirred at room temperature overnight, water was added and the product extracted with Et_2O. The organic phase was washed (10% $Na_2S_2O_3$, then water), dried ($MgSO_4$), filtered, and evaporated to obtain the desired iodide as a slightly yellow oil that was used without further purification.

*(A) Benzyl-(2-iodoethyl)ether (**5a**) (45, 54−59):* 93%. ^{1}H NMR δ 7.35−7.40 (m, 5H), 4.60 (s, 2H), 3.76 (t, 2H, J = 6.6 Hz), 3.30 (t, 2H, J = 6.6 Hz); ^{13}C NMR δ 138.09, 128.80, 128.17, 128.09, 73.19, 71.04, 3.40.

*(B) Benzyl-(3-iodopropyl)ether (**5b**) (45, 60−62):* 95%. ^{1}H NMR δ 7.33−7.37 (m, 5H), 4.53 (s, 2H), 3.56 (t, 2H, J = 5.4 Hz), 3.32 (t, 2H, J = 6.2 Hz), 2.03−2.16 (m, 2H); ^{13}C NMR δ 138.52, 128.74, 127.99, 73.45, 69.92, 33.83, 3.91.

*(C) Benzyl-(4-iodobutyl)ether (**5c**) (50, 51, 63−66):* 90%. ^{1}H NMR δ 7.30−7.38 (m, 5H), 4.52 (s, 2H), 3.51 (t, 2H, J = 6.0 Hz), 3.22 (t, 2H, J = 6.6 Hz), 1.68−2.02 (m, 4H); ^{13}C NMR δ 138.71, 129.13, 128.72, 127.92, 73.26, 69.34, 30.96, 30.72, 7.27.

*(D) Benzyl-(5-iodopentyl)ether (**5d**) (67, 68):* 98%. ^{1}H NMR δ 7.25−7.40 (m, 5H), 4.52 (s, 2H), 3.49 (t, 2H, J = 6.5 Hz), 3.20 (t, 2H, J = 7.0 Hz), 1.83−1.90 (m, 2H), 1.60−1.70 (m, 2H), 1.50−1.55 (m, 2H); ^{13}C NMR δ 138.90, 128.73, 127.98, 127.90, 73.29, 70.36, 33.70, 29.06, 27.62, 7.21.

*(E) Benzyl-(6-iodopentyl)ether (**5e**) (63, 66):* 82%. ^{1}H NMR δ 7.29−7.35 (m, 5H), 4.50 (s, 2H), 3.47 (t, 2H, J = 6.4 Hz), 3.18 (t, 2H, J = 6.8 Hz), 1.35−1.90 (m, 8H); ^{13}C NMR δ 139.02, 128.77, 128.02, 127.90, 73.30, 70.59, 33.87, 30.71, 29.97, 25.60, 7.51.

*General Procedure for Ketones **6a**−**e**.* To a solution of ethylacetoacetate sodium salt (22.0 g, 144.6 mmol) in anhydrous DME (200 mL) at room temperature was added a solution of the iodide **5a**−**e** (72.3 mmol) in anhydrous DME (50 mL), and the reaction mixture was heated at reflux overnight. After cooling to room temperature, a solution of NaOH (16.0 g, 400.0 mmol) in water (160 mL) was added, and the mixture was refluxed for 2 h, cooled to room temperature, acidified with 50% H_2SO_4 (40 mL, final pH ∼2), and then refluxed for 2 h more. Water was added, and the product was extracted with Et_2O. The organic phase was washed (10% $NaHCO_3$ then water), dried ($MgSO_4$), filtered, and evaporated to obtain an oily residue. Purification by distillation under reduced pressure gave the ketone as a colorless oil.

*(A) 5-Benzyloxy-2-pentanone (**6a**) (69−71):* bp 98−100 °C/0.7 mmHg (79%). ^{1}H NMR δ 7.32−7.36 (m, 5H), 4.49

(s, 2H), 3.49 (t, 2H, $J = 6.0$ Hz), 2.56 (t, 2H, $J = 7.2$ Hz), 2.14 (s, 3H), 1.62−1.95 (m, 2H); ^{13}C NMR δ 208.93, 138.70, 128.68, 127.93, 127.88, 73.17, 69.58, 40.64, 30.31, 24.20.

*(B) 6-Benzyloxy-2-hexanone (**6b**) (72, 73):* bp 108−110 °C/0.7 mmHg (77%). ^{1}H NMR δ 7.26−7.38 (m, 5H), 4.43 (s, 2H), 3.41 (t, 2H, $J = 6.2$ Hz), 2.38 (t, 2H, $J = 7.0$ Hz), 2.06 (s, 3H), 1.50−1.65 (m, 4H); ^{13}C NMR δ 209.23, 138.92, 128.73, 128.01, 127.90, 73.29, 70.34, 43.76, 30.22, 29.54, 20.98.

*(C) 7-Benzyloxy-2-heptanone (**6c**) (74):* bp 120−125 °C/0.7 mmHg (73%). ^{1}H NMR δ 7.30−7.36 (m, 5H), 4.50 (s, 2H), 3.48 (t, 2H, $J = 6.2$ Hz), 2.44 (t, 2H, $J = 7.2$ Hz), 2.14 (s, 3H), 1.32−1.70 (m, 6H); ^{13}C NMR δ 209.62, 138.98, 128.74, 128.10, 127.90, 73.22, 70.45, 43.95, 30.15, 29.81, 26.05, 23.86.

*(D) 8-Benzyloxy-2-octanone (**6d**):* bp 135−140 °C/0.7 mmHg (66%). ^{1}H NMR δ 7.25−7.35 (m, 5H), 4.50 (s, 2H), 3.47 (t, 2H, $J = 6.5$ Hz), 2.42 (t, 2H, $J = 7.5$ Hz), 2.13 (s, 3H), 1.52−1.65 (m, 4H), 1.30−1.42 (m, 4H); ^{13}C NMR δ 209.46, 139.00, 128.67, 127.93, 127.80, 73.20, 70.64, 44.00, 30.15, 29.92, 29.31, 26.33, 24.10. LRMS (EI): (M^+) 234.2.

*(E) 9-Benzyloxy-2-nonanone (**6e**):* bp 135−140 °C/0.3 mmHg (79%). ^{1}H NMR δ 7.26−7.35 (m, 5H), 4.48 (s, 2H), 3.45 (t, 2H, $J = 6.6$ Hz), 2.39 (t, 2H, $J = 7.4$ Hz), 2.16 (s, 3H), 1.30−1.62 (m, 10H); ^{13}C NMR δ 209.53, 139.00, 128.65, 127.92, 127.78, 73.19, 70.33, 44.08, 30.18, 30.03, 29.55, 29.44, 26.37, 24.12. LRMS (EI): (M^+) 248.2.

*General Procedure for Olefins **7a**−**e**.* Triethylphosphonoacetate (100.0 mmol, 22.4 g) was added dropwise to a stirred suspension of NaH (100.0 mmol, 2.4 g) in dry THF (60 mL) at 0 °C and allowed to stir for 30 min. A solution of the ketone **6a**−**e** (50.0 mmol) in dry THF (40 mL) was then added at the same temperature. After the reaction was allowed to warm to room temperature and stirred overnight, it was then diluted with saturated NH_4Cl and extracted with Et_2O. The ether layer was washed with water, dried ($MgSO_4$), filtered, and evaporated to give an oily residue. Purification by distillation under reduced pressure yields the olefin as a colorless oil and as an *E*/*Z* mixture in the ratio ∼8:2. The distillate was further purified by flash chromatography (5% Et_2O in hexane) to enrich the *E* isomer. Evaporation of the last fractions afforded an *E*/*Z* mixture in the ratio 9:1.

*(A) Ethyl-6-benzyloxy-3-methyl-2-hexenoate (**7a**) (71):* bp 130−140 °C/0.7 mmHg (72% after distillation, 46% after flash). ^{1}H NMR (*E*) δ 7.27−7.35 (m, 5H), 5.66−5.68 (m, 1H), 4.49 (s, 2H), 4.08−4.19 (m, 2H), 3.43−3.51 (m, 2H), 2.19−2.30 (m, 2H), 2.15 (d, 3H, $J = 1.2$ Hz), 1.72−1.90 (m, 2H), 1.23−1.30 (m, 3H); ^{13}C NMR (*E*) δ 167.80, 160.18, 138.83, 128.79, 128.04, 128.00, 116.20, 73.30, 69.76, 59.80, 37.77, 27.81, 19.00, 14.60. ^{1}H NMR (*Z*) δ 7.27−7.35 (m, 5H), 5.66−5.68 (m, 1H), 4.50 (s, 2H), 4.08−4.19 (m, 2H), 3.43−3.51 (m, 2H), 2.66−2.74 (m, 2H), 1.88 (d, 3H, $J = 1.2$ Hz), 1.72−1.90 (m, 2H), 1.23−1.30 (m, 3H); ^{13}C NMR (*Z*) δ 167.80, 160.18, 138.83, 128.79, 128.04, 128.00, 116.25, 73.30, 70.64, 59.80, 30.44, 28.05, 25.80, 22.07.

*(B) Ethyl-7-benzyloxy-3-methyl-2-heptenoate (**7b**) (49):* bp 140−150 °C/0.7 mmHg (62% after distillation, 50% after flash). ^{1}H NMR (*E*) δ 7.20−7.28 (m, 5H), 5.59−5.60 (m, 1H), 4.43 (s, 2H), 4.03−4.10 (m, 2H), 3.38−3.44 (m, 2H), 2.07−2.10 (m, 2H), 2.09 (d, 3H, $J = 1.0$ Hz), 1.48−1.65 (m, 4H), 1.19−1.23 (m, 3H); ^{13}C NMR (*E*) δ 167.17, 160.07, 138.90, 128.72, 127.96, 127.88, 116.09, 73.28, 70.30, 59.78, 40.96, 29.62, 24.39, 19.00, 14.68. ^{1}H NMR (*Z*) δ 7.20−7.28 (m, 5H), 5.59−5.60 (m, 1H), 4.44 (s, 2H), 4.03−4.10 (m, 2H), 3.38−3.44 (m, 2H), 2.57−2.61 (m, 2H), 1.81 (d, 3H, $J = 1.5$ Hz), 1.48−1.65 (m, 4H), 1.19−1.23 (m, 3H); ^{13}C NMR (*Z*) δ 166.92, 160.32, 138.90, 128.72, 127.96, 127.88, 116.38, 73.28, 70.45, 59.78, 40.96, 32.60, 30.10, 25.20, 25.05.

*(C) Ethyl-8-benzyloxy-3-methyl-2-octenoate (**7c**):* bp 155−165 °C/0.7 mmHg (81% after distillation, 50% after flash). ^{1}H NMR (*E*) δ 7.20−7.27 (m, 5H), 5.57−5.58 (m, 1H), 4.43 (s, 2H), 4.01−4.09 (m, 2H), 3.38−3.41 (m, 2H), 2.04−2.08 (m, 2H), 2.07 (d, 3H, $J = 1.5$ Hz), 1.53−1.60 (m, 2H), 1.29−1.45 (m, 4H), 1.18−1.22 (m, 3H); ^{13}C NMR (*E*) δ 167.21, 160.33, 138.96, 128.70, 127.97, 127.85, 115.92, 73.25, 70.53, 59.78, 41.20, 29.91, 27.57, 26.18, 19.05, 14.68. ^{1}H NMR (*Z*) δ 7.20−7.27 (m, 5H), 5.57−5.58 (m, 1H), 4.43 (s, 2H), 4.01−4.09 (m, 2H), 3.38−3.41 (m, 2H), 2.53−2.57 (m, 2H), 1.80 (d, 3H, $J = 1.0$ Hz), 1.53−1.60 (m, 2H), 1.29−1.45 (m, 4H), 1.18−1.22 (m, 3H); ^{13}C NMR (*Z*) δ 166.96, 160.58, 138.96, 128.70, 127.97, 127.85, 116.21, 73.25, 70.53, 59.78, 41.20, 33.80, 32.00, 28.10, 19.20, 14.58. LRMS (EI): (M^+) 290.3.

*(D) Ethyl-9-benzyloxy-3-methyl-2-nonenoate (**7d**):* bp 172−176 °C/0.7 mmHg (90% after distillation, 48% after flash). ^{1}H NMR (*E*) δ 7.27−7.36 (m, 5H), 5.64−5.67 (m, 1H), 4.51 (s, 2H), 4.10−4.19 (m, 2H), 3.46−3.49 (m, 2H), 2.11−2.16 (m, 2H), 2.15 (d, 3H, $J = 1.0$ Hz), 1.55−1.67 (m, 2H), 1.26−1.50 (m, 9H); ^{13}C NMR (*E*) δ 167.19, 160.44, 139.01, 128.67, 127.93, 127.80, 115.84, 73.20, 70.66, 59.74, 41.18, 29.98, 29.33, 27.64, 26.39, 19.02, 14.67. ^{1}H NMR (*Z*) δ 7.27−7.36 (m, 5H), 5.64−5.67 (m, 1H), 4.51 (s, 2H), 4.10−4.19 (m, 2H), 3.46−3.49 (m, 2H), 2.60−2.64 (m, 2H), 1.88 (d, 3H, $J = 1.5$ Hz), 1.55−1.67 (m, 2H), 1.26−1.50 (m, 9H); ^{13}C NMR (*Z*) δ 166.96, 160.69, 139.01, 128.67, 127.93, 127.80, 116.04, 73.20, 70.66, 59.74, 41.20, 33.66, 29.91, 28.20, 27.76, 19.02, 14.67. LRMS (EI): (M^+) 304.3.

*(E) Ethyl-10-benzyloxy-3-methyl-2-decenoate (**7e**):* bp 163−168 °C/0.3 mmHg (88% after distillation, 54% after flash). ^{1}H NMR (*E*) δ 7.27−7.40 (m, 5H), 5.66−5.68 (m, 1H), 4.52 (s, 2H), 4.10−4.22 (m, 2H), 3.44−3.51 (m, 2H), 2.08−2.18 (m, 2H), 2.16 (d, 3H, $J = 1.0$ Hz), 1.25−1.70 (m, 13H); ^{13}C NMR (*E*) δ 167.28, 160.65, 139.07, 128.72, 127.99, 127.85, 115.84, 73.26, 70.80, 59.80, 41.29, 30.10, 29.63, 29.50, 27.69, 26.46, 19.09, 14.72. ^{1}H NMR (*Z*) δ 7.27−7.40 (m, 5H), 5.66−5.68 (m, 1H), 4.52 (s, 2H), 4.10−4.22 (m, 2H), 3.44−3.51 (m, 2H), 2.58−2.66 (m, 2H), 1.88 (d, 3H, $J = 1.0$ Hz), 1.25−1.70 (m, 13H); ^{13}C NMR (*Z*) δ 166.88, 160.80, 139.07, 128.72, 127.99, 127.85, 116.37, 73.26, 70.80, 59.80, 41.29, 33.71, 30.10, 29.63, 28.10, 25.50, 19.09, 14.72. LRMS (EI): (M^+) 318.4.

*General Procedure for Ester Reduction To Afford Alcohols **8a**−**e**.* A solution of the olefin **7a**−**e** (7.5 mmol) in dry THF (10 mL) was added to a suspension of $LiAlH_4$ (303.6 mg, 8.0 mmol) in dry THF (20 mL) at 0 °C. The reaction was allowed to warm to room temperature and stirred for 2 h. After addition of EtOAc, the reaction was diluted with water and extracted with Et_2O. The ether layer was washed with water, dried ($MgSO_4$), filtered, and evaporated to give an oily residue that was purified by flash chromatography (20% EtOAc in hexane).

*(A) 6-Benzyloxy-3-methyl-2-hexen-1-ol (**8a**) (71):* 60%. ^{1}H NMR (*E*) δ 7.29−7.40 (m, 5H), 5.40−5.49 (m, 1H), 4.54

(s, 2H), 4.17 (d, 2H, $J = 8.0$ Hz), 3.51 (t, 2H, $J = 6.6$ Hz), 2.10−2.19 (m, 2H), 1.63−1.82 (m, 6H); ^{13}C NMR (*E*) δ 139.63, 138.97, 128.78, 128.09, 127.96, 124.02, 73.24, 70.15, 59.66, 36.28, 28.02, 16.48.

*(B) 7-Benzyloxy-3-methyl-2-hepten-1-ol (**8b**):* 53%. ^{1}H NMR (*E*) δ 7.27−7.39 (m, 5H), 5.39−5.50 (m, 1H), 4.55 (s, 2H), 4.17 (d, 2H, $J = 7.0$ Hz), 3.52 (t, 2H, $J = 6.0$ Hz), 2.03−2.17 (m, 2H), 1.53−1.77 (m, 8H); ^{13}C NMR (*E*) δ 139.80, 139.00, 128.76, 128.04, 127.92, 123.97, 73.23, 70.56, 59.63, 39.55, 29.61, 24.50, 16.39. LRMS (EI): (M^+) 234.2.

*(C) 8-Benzyloxy-3-methyl-2-octen-1-ol (**8c**):* 58%. ^{1}H NMR (*E*) δ 7.27−7.37 (m, 5H), 5.35−5.47 (m, 1H), 4.52 (s, 2H), 4.15 (d, 2H, $J = 7.0$ Hz), 3.48 (t, 2H, $J = 6.2$ Hz), 1.99−2.07 (m, 2H), 1.28−1.70 (m, 10H); ^{13}C NMR (*E*) δ 140.20, 138.98, 128.70, 127.99, 127.85, 123.68, 73.23, 70.72, 59.71, 39.80, 29.97, 27.81, 26.19, 16.49. LRMS (EI): (M^+) 248.2.

*(D) 9-Benzyloxy-3-methyl-2-nonen-1-ol (**8d**):* 54%. ^{1}H NMR (*E*) δ 7.27−7.36 (m, 5H), 5.39−5.42 (m, 1H), 4.52 (s, 2H), 4.15 (d, 2H, $J = 7.0$ Hz), 3.48 (t, 2H, $J = 6.5$ Hz), 1.99−2.04 (m, 2H), 1.60−1.67 (m, 5H), 1.30−1.45 (m, 7H); ^{13}C NMR (*E*) δ 140.45, 139.08, 128.72, 128.00, 127.86, 123.60, 73.24, 70.82, 59.78, 39.84, 30.08, 29.48, 27.96, 26.46, 16.53. LRMS (EI): (M^+) 262.2.

*(E) 10-Benzyloxy-3-methyl-2-decen-1-ol (**8e**):* 56%. ^{1}H NMR (*E*) δ 7.28−7.38 (m, 5H), 5.38−5.46 (m, 1H), 4.52 (s, 2H), 4.16 (d, 2H, $J = 7.0$ Hz), 3.48 (t, 2H, $J = 6.6$ Hz), 1.97−2.08 (m, 2H), 1.58−1.68 (m, 5H), 1.22−1.48 (m, 9H); ^{13}C NMR (*E*) δ 140.10, 139.05, 128.72, 128.01, 127.85, 123.50, 73.23, 70.85, 59.78, 39.87, 30.12, 29.71, 29.57, 27.95, 26.51, 16.54. LRMS (EI): (M^+) 276.2.

*Ester Reduction of **7c** Using DIBAL-H To Afford Alcohol **8c**.* To the solution of ester **7c** (5.50 g, 18.9 mmol) in 100 mL of dry THF was added diisobutyl aluminum hydride (1.0 M solution in toluene, 50.3 mL, 75.5 mmol) under argon at −78 °C. The reaction was stirred at −78 °C for 2 h. Methanol was added, and the reaction mixture was allowed to warm to room temperature. After dilution with water, the mixture was extracted with Et_2O (2×). The combined organic layers were washed (water then brine) and dried over $MgSO_4$. Concentration followed by flash chromatography purification (20% EtOAc in hexane) afforded 4.50 g (95.9%) of alcohol **8c** as a colorless oil.

*General Procedure for Conversion of Alcohols **8a**−**e** into Pyrophosphates **1a**−**e**.* To a solution of alcohol **8a**−**e** (1.15 mmol) in dry acetonitrile (10 mL) was added *N*,*N*-diisopropylethylamine (230.5 mg, 1.83 mmol), and the solution was then placed at 0 °C with stirring. After 10 min at 0 °C, PPh_3-Cl_2 (547.5 mg, 1.71 mmol) was added evenly to the reaction mixture over a period of 10 min. The reaction was stirred at 0 °C for 40 min, then diluted with 20 mL of 10% EtOAc in hexane, and filtered over a short pad of silica gel. The filtrate was concentrated to afford a crude oily residue which was then dissolved in 6 mL of dry acetonitrile. Tris(tetrabutylammonium)hydrogen pyrophosphate (2.23 mmol, 2.28 g) was added, and the reaction mixture was stirred for 3 h at room temperature. Solvent was removed, and the residue was dissolved in 3 mL of ion exchange buffer (25 mM NH_4HCO_3 in 2% v/v *i*-PrOH−water). The solution was loaded onto a cation-exchange resin (NH_4^+ form) and eluted with ion exchange buffer, and the eluant was lyophilized. The crude ammonium salt was purified by RP-HPLC to give the pyrophosphates **1a**−**e** as white solids.

*(A) 6-Benzyloxy-3-methyl-2-hexen-1-ol pyrophosphate (**1a**):* 78%. HPLC: $t_R \approx 12.8$ min. ^{1}H NMR (D_2O, 400 MHz) δ 7.48−7.38 (m, 5H), 5.47 (tq, 1H, $J = 1.1$ Hz), 4.56 (s, 2H), 4.48 (t, 2H, $J = 6.6$ Hz), 3.58 (t, 2H, $J = 6.8$ Hz), 2.13 (t, 2H, $J = 7.9$ Hz), 1.79−1.75 (m, 2H), 1.72 (s, 3H); ^{13}C NMR (D_2O, 100.7 MHz) δ 144.96, 140.32, 131.59, 131.47, 131.14, 122.94 (m), 75.38, 72.69, 65.47 (d, $J = 5.3$ Hz), 38.08, 29.52, 18.35; ^{31}P NMR (D_2O, 162.1 MHz) δ −6.93 (d, 1P, $J = 22$ Hz), −9.48 (d, 1P, $J = 22$ Hz). HRMS (MALDI): calculated $(M-H)^-$ 379.072, measured 379.071.

*(B) 7-Benzyloxy-3-methyl-2-hepten-1-ol pyrophosphate (**1b**):* 81%. HPLC: $t_R \approx 13.5$ min. ^{1}H NMR (D_2O, 400 MHz) δ 7.49−7.37 (m, 5H), 5.46 (tq, 1H, $J = 1.3$ Hz), 4.56 (s, 2H), 4.49 (t, 2H, $J = 6.6$ Hz), 3.59 (t, 2H, $J = 6.6$ Hz), 2.08 (t, 2H, $J = 7.3$ Hz), 1.71 (s, 3H), 1.65−1.55 (m, 2H), 1.54−1.44 (m, 2H); ^{13}C NMR (D_2O, 100.7 MHz) δ 145.89, 140.34, 131.58, 131.44, 131.12, 122.58 (m), 75.30, 72.99, 65.57 (d, $J = 5.3$ Hz), 41.26, 31.02, 26.20, 18.30; ^{31}P NMR (D_2O, 162.1 MHz) δ −7.36 (d, 1P, $J = 21$ Hz), −9.44 (d, 1P, $J = 21$ Hz). HRMS (MALDI): calculated $(M-H)^-$ 393.087, measured 393.087.

*(C) 8-Benzyloxy-3-methyl-2-octen-1-ol pyrophosphate (**1c**):* 78%. HPLC: $t_R \approx 14.0$ min. ^{1}H NMR (D_2O, 400 MHz) δ 7.48−7.38 (m, 5H), 5.46 (tq, 1H, $J = 1.3$ Hz), 4.55 (s, 2H), 4.49 (t, 2H, $J = 6.4$ Hz), 3.57 (t, 2H, $J = 6.6$ Hz), 2.06 (t, 2H, $J = 7.7$ Hz), 1.71 (s, 3H), 1.62 (p, 2H, $J = 7.5$ Hz), 1.44 (p, 2H, $J = 7.3$ Hz), 1.33 (p, 2H, $J = 6.8$ Hz); ^{13}C NMR (D_2O, 100.7 MHz) δ 146.29, 140.36, 131.57, 131.41, 131.11, 122.30 (m), 75.28, 73.11, 65.56 (d, $J = 5.3$ Hz), 41.58, 31.28, 29.40, 27.77, 18.39; ^{31}P NMR (D_2O, 162.1 MHz) δ −7.28 (d, 1P, $J = 22$ Hz), −9.46 (d, 1P, $J = 21$ Hz). HRMS (MALDI): calculated $(M-H)^-$ 407.103, measured 407.102.

*(D) 9-Benzyloxy-3-methyl-2-nonen-1-ol pyrophosphate (**1d**):* 77%. HPLC: $t_R \approx 14.6$ min. ^{1}H NMR (D_2O, 400 MHz) δ 7.48−7.38 (m, 5H), 5.45 (tq, 1H, $J = 1.3$ Hz), 4.55 (s, 2H), 4.49 (t, 2H, $J = 6.6$ Hz), 3.57 (t, 2H, $J = 6.8$ Hz), 2.06 (t, 2H, $J = 7.5$ Hz), 1.71 (s, 3H), 1.60 (p, 2H, $J = 7.5$ Hz), 1.43 (p, 2H, $J = 7.7$ Hz), 1.35 (m, 2H), 1.29 (m, 2H); ^{13}C NMR (D_2O, 100.7 MHz) δ 146.71, 140.34, 131.57, 131.44, 131.11, 121.99 (m), 75.30, 73.19, 65.80 (d, $J = 5.3$ Hz), 41.63, 31.36, 30.93, 29.62, 27.96, 18.37; ^{31}P NMR (D_2O, 162.1 MHz) δ −9.09 (d, 1P, $J = 21$ Hz), −9.67 (d, 1P, $J = 20$ Hz). HRMS (MALDI): calculated $(M-H)^-$ 421.119, measured 421.118.

*(E) 10-Benzyloxy-3-methyl-2-decen-1-ol pyrophosphate (**1e**):* 78%. HPLC: $t_R \approx 15.1$ min. ^{1}H NMR (D_2O, 400 MHz) δ 7.48−7.38 (m, 5H), 5.46 (tq, 1H, $J = 1.3$ Hz), 4.56 (s, 2H), 4.48 (t, 2H, $J = 6.6$ Hz), 3.58 (t, 2H, $J = 6.6$ Hz), 2.06 (t, 2H, $J = 7.7$ Hz), 1.72 (s, 3H), 1.60 (p, 2H, $J = 7.0$ Hz), 1.43 (p, 2H, $J = 7.3$ Hz), 1.38−1.24 (m, 6H); ^{13}C NMR (D_2O, 100.7 MHz) δ 146.49, 140.36, 131.58, 131.45, 131.13, 122.36 (m), 75.30, 73.22, 65.36 (d, $J = 5.3$ Hz), 41.72, 31.41, 31.23, 31.12, 29.71, 28.01, 18.43; ^{31}P NMR (D_2O, 162.1 MHz) δ −5.48 (d, 1P, $J = 22$ Hz), −9.31 (d, 1P, $J = 22$ Hz). HRMS (MALDI): calculated $(M-H)^-$ 435.134, measured 435.134.

Continuous Fluorescence Assay. The kinetic constants K_m, V_{max}, and k_{cat} for FPP, GPP, and BnPP analogues **1a**−**e** were determined using the continuous spectrofluorometric assay

originally developed by Pompliano et al. (*75*) and modified by Poulter and co-workers (*76*) with some additional modification. Utilizing *N*-dansyl-GCVLS as the peptide substrate, the linear portion of the increase in fluorescence versus time was measured with a Hitatchi F2000 spectrofluorometer (excitation wavelength 350 nm; emission wavelength 505 nm). The assay components {209.6 μL of assay buffer (50 mM Tris-HCl, pH 7.5, 5 mM DTT, 5 mM $MgCl_2$, 10 μM $ZnCl_2$), 40 μL of detergent solution (0.4% *n*-dodecyl-β-D-maltoside in H_2O), 0.4 μL of *N*-dansyl-GCVLS solution (1 mM in 20 mM Tris-HCl, pH 7.5, 10 mM EDTA), 100 μL of FPP or FPP analogue (2−20 mM stock solutions in 12 mM NH_4HCO_3/MeOH (7:3 v/v), final concentration 0.03−3 μM} were assembled in a 1.5 mL Eppendorf tube in the order indicated above and incubated at 30 °C for 5 min. Rat protein farnesyltransferase, recombinantly expressed in *E. coli* (*77*) containing an N-terminal His-tag on the β-subunit, was a gift from Jennifer Pickett and Carol Fierke (University of Michigan). A 50 μL FTase solution [0.1 mg/mL BSA with 0.27 μM FTase (for FPP only) or 1.2 μM FTase in assay buffer] was loaded into a 1.0 mL quartz cuvette and incubated at 30 °C for 5 min. The reaction was initiated by the addition of the 350 μL assay buffer/peptide/prenyl pyrophosphate solution to the 50 μL FTase/BSA solution. Fluorescence was detected using a time-based scan at 30 °C for a period of 60 s. The velocity was determined by converting the rate of increase in fluorescence intensity units (FLU/s) to pmol/s by fitting the data to eq 1:

$$V = (R \times P)/F_{max} \quad (1)$$

where V is the velocity of the reaction in pmol/s, R is the rate of the reaction in FLU/s, and P is equal to the number of picomoles of FPP, GPP, or FPP analogues **1a**−**e** used in the reaction mixture when the number of *N*-dansyl-GCVLS picomoles is 2-fold or greater than the number of prenyl pyrophosphate picomoles. F_{max} is the fluorescence intensity of the reaction mixture after incubation for 60 min at 30 °C when an amount of P was used for FPP, GPP, or FPP analogues **1a**−**e**. Based on HPLC analysis of large-scale reactions under similar conditions, we assume that each reaction has gone to completion.

Product Studies. Large-scale reactions contained 50 mM Tris·HCl, pH 7.5, 5 mM $MgCl_2$, 10 μM $ZnCl_2$, 5 mM DTT, 0.04% *n*-dodecyl-β-D-maltoside, 2.5 μM *N*-dansyl-GCVLS, 0.25 μM FTase, and 25 μM FPP, GPP, or **1a**−**e** in a final reaction volume of 400 μL. After the samples were allowed to react for 1 h at 37 °C, each reaction mixture was loaded onto an analytical Vydac C_8 (208TP54) column and eluted with a linear gradient of 0−40 min 10% B to 100% B at a flow rate of 1 mL/min. Solvents: A = 0.01% (v/v) TFA in water; B = 0.01% (v/v) TFA in CH_3CN. The fraction corresponding to coincident absorbance and fluorescence peaks was collected and analyzed by mass spectroscopy.

*(A) N-Dansyl-G-(farnesyl-1-S-cysteine)-VLS (**9**):* HPLC: $t_R \approx 27.1$ min. HRMS (ESI): calculated for $C_{46}H_{71}N_6O_9S_2$ 915.4724, measured 915.4726.

*(B) N-Dansyl-G-(geranyl-1-S-cysteine)-VLS (**10**):* HPLC: $t_R \approx 22.6$ min. HRMS (ESI): calculated for $C_{41}H_{63}N_6O_9S_2$ 847.4098, measured 847.4095.

*(C) N-Dansyl-G-(6-benzyloxy-3-methyl-2-hexen-1-S-cysteine)-VLS (**11a**):* HPLC: $t_R \approx 21.9$ min. HRMS (ESI): calculated for $C_{45}H_{65}N_6O_{10}S_2$ 913.4204, measured 913.4186.

*(D) N-Dansyl-G-(7-benzyloxy-3-methyl-2-hepten-1-S-cysteine)-VLS (**11b**):* HPLC: $t_R \approx 22.8$ min. HRMS (ESI): calculated for $C_{46}H_{67}N_6O_{10}S_2$ 927.4360, measured 927.4341.

*(E) N-Dansyl-G-(8-benzyloxy-3-methyl-2-octen-1-S-cysteine)-VLS (**11c**):* HPLC: $t_R \approx 23.8$ min. HRMS (ESI): calculated for $C_{47}H_{69}N_6O_{10}S_2$ 941.4517, measured 941.4495.

*(F) N-Dansyl-G-(9-benzyloxy-3-methyl-2-nonen-1-S-cysteine)-VLS (**11d**):* HPLC: $t_R \approx 24.9$ min. HRMS (ESI): calculated for $C_{48}H_{71}N_6O_{10}S_2$ 955.4673, measured 955.4643.

*(G) N-Dansyl-G-(10-benzyloxy-3-methyl-2-decen-1-S-cysteine)-VLS (**11e**):* HPLC: $t_R \approx 25.9$ min. HRMS (ESI): calculated for $C_{49}H_{73}N_6O_{10}S_2$ 969.4830, measured 969.4819.

Molecular Modeling. The FTase starting structure was created by adding hydrogen atoms to the binary FTase−FPP crystal structure (PDB code 1FT2) (*24*). Atom potential types and partial charges were assigned based on the cff91 force field defaults. The cysteine and histidine residues coordinating the zinc atom were considered to be deprotonated, and their charges were modified accordingly. Since charges for the deprotonated residues are not provided in the cff91 force field library, charges for deprotonated cysteine were taken from the AMBER 6.0 library, and charges for deprotonated histidine (histidinate) were taken from Pang et al. (*78*) Isoprenoid and BnPP molecules were constructed in the "Builder" module of Insight II (v2000, MSI, Inc.). Their atom potential types and partial charges were assigned automatically based on hybridization and connectivities, resulting in an overall charge of −2.5. To bring the charge down to the proper value of −3, the partial charges of the pyrophosphate groups were modified to more closely resemble those calculated by RESP (*79*) fitting of FPP (Y. P. Pang, personal communication). All ligand starting structures were in the fully extended conformation. Minimization and molecular dynamics were set up using the "Docking" module and carried out with the "CDiscover" module of Insight II (v2000, MSI, Inc.) under the cff91 force field. The coordinates of all protein residues were fixed, except for the following active site residues, which were allowed to move: Tyr 200α, His 201α, Trp 102β, Ala 151β, Tyr 154β, Met 193β, Asp 200β, Arg 202β, Tyr 205β, Cys 206β, Gly 250β, Tyr 251β, Phe 253β, Cys 254β, Trp 303β, Tyr 361β, Tyr 365β. Residues that coordinate the oxygen atoms of the pyrophosphate moiety were initially allowed to move, but this allowed too much distortion of the active site, so these residues were subsequently held fixed. For similar reasons, residues that coordinate the zinc atom were also fixed, as was the zinc atom itself. A two-stage refinement was used to model the binary complexes. The first round consisted of a Monte Carlo conformational search and minimization, from which 20 structures were generated. This was done with the electrostatic component of the force field turned off and the van der Waals component scaled to 10%. The second round consisted of a Monte Carlo conformational search and minimization of the 20 structures with all components of the force field at 100% and inclusion of a distance-dependent dielectric component (dielectric constant = 1) followed by simulated annealing consisting of 50 increments of 100 fs each to cool the system from 500 to 300 K. The overall and per residue binding energy of each of the 20 structures was then measured via a CDiscover routine in order to determine the most likely binding mode for each ligand. For comparison to these generated structures, the modified 1FT2 binary

Scheme 1[a]

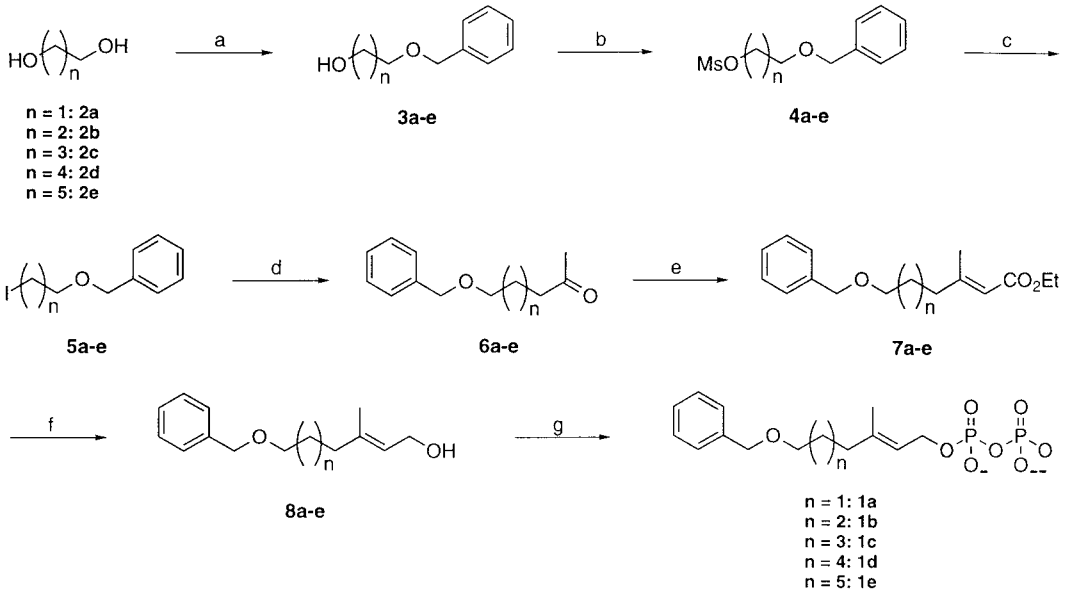

[a] Reaction conditions: (a) benzyl chloride, KOH; (b) MsCl, pyridine; (c) NaI, acetone; (d) sodium ethylacetoacetate; (e) $(EtO)_2POCH_2CO_2Et$, NaH, THF; (f) $LiAlH_4$ or DIBAL-H, THF; (g) 1. Ph_3PCl_2, 2. $\{(n\text{-}Bu)_4N\}_3HP_2O_7$, CH_3CN.

cocrystal structure was also minimized as in the second round of refinement, but no simulated annealing was performed.

RESULTS AND DISCUSSION

Synthesis of Benzylalkyl Pyrophosphate Analogues of FPP. Analogues **1a**−**e** were synthesized in seven steps starting from the commercially available glycols **2a**−**e** as outlined in Scheme 1. An attractive feature of this path is that the overall length of the analogues **1a**−**e** is easily varied by employing different starting alkyl diols. An excess of the appropriate diol **2a**−**e** was monobenzylated with benzyl chloride and KOH to provide the monoethers **3a**−**e** in 62−71% yield after distillation. Alcohols **3a**−**e** were transformed into mesylates **4a**−**e** by standard procedures with methanesulfonyl chloride and pyridine. The mesylates **4a**−**e** were then transformed into iodides **5a**−**e** in high yield via the Finkelstein reaction. Ketones **6a**−**e** were obtained in 66−79% yield after distillation by reacting iodides **5a**−**e** with sodium ethylacetoacetate followed by saponification of the ester and subsequent decarboxylation. Attempts to form ketones **6a**−**e** directly from mesylates **4a**−**e** with either the sodium salt of ethylacetoacetate or salts formed from ethylacetoacetate and LHMDS, KHMDS, or DBU resulted in poor yield of the desired product. Condensation of ketones **6a**−**e** with sodium triethylphosphonoacetate afforded olefins **7a**−**e** in 62−90% yield after distillation. Analysis of the ^1H NMR spectra indicated that olefins **7a**−**e** were a mixture of *E*/*Z* isomers in a 4:1 ratio. Resonances for the *E* and *Z* isomers of the esters **7a**−**e** were assigned via NOE experiments. Alternative reaction conditions for the Horner−Wadworth−Emmons condensation did not alter the *E*/*Z* ratio.[2] We found chromatographic separation of the desired *E* isomer from the *Z* isomer to be very difficult at all levels of the synthesis. Repeated flash chromatography of the ester isomer mixture **7a**−**e** raised the *E*/*Z* mixture to a 9:1 ratio. This *E*/*Z* mixture was carried through the remainder of the synthesis.

Reduction of esters **7a**−**e** with lithium aluminum hydride furnished the allylic alcohols **8a**−**e** in 53−60% yield. We found that the saturated alcohol formed by LAH overreduction was the major byproduct of this reaction. However, the desired alcohol **8c** could be obtained in 96% yield by reduction of ester **7c** with DIBAL-H. Alcohols **8a**−**e** were converted into their corresponding allylic chlorides using Ph_3PCl_2 as previously described (*18*), and immediately pyrophosphorylated with $(n\text{-}Bu_4N)_3HP_2O_7$ (*83*, *84*). Purification of the reaction mixture by ion exchange chromatography and reverse phase HPLC provided the FPP analogues **1a**−**e** as white solids.

*Analogues **1a**−**e**, FPP, and GPP, but Not GGPP, Are Substrates for Farnesyltransferase in Vitro.* A continuous fluorescence assay using the peptide *N*-dansyl-GCVLS was employed to determine whether compounds **1a**−**e** were substrates or inhibitors for recombinant rat FTase. The continuous fluorescence assay, first developed by Pompliano et al. for the human FTase enzyme (*75*) and adapted by Poulter and co-workers for the yeast FTase enzyme (*76*), monitors the time-dependent increase in the fluorescence of the dansyl group due to the increase in the local hydrophobic environment as the adjacent cysteine residue is isoprenylated. A time-dependent increase in fluorescence was observed when FPP, GPP, and analogues **1a**−**e** were incubated with FTase and *N*-dansyl-GCVLS peptide substrate, indicating all of the analogues were substrates for FTase. However, no increase in fluorescence was observed when GGPP was used, in agreement with previously published reports that GGPP is not a substrate for FTase (*21*, *22*).

HPLC and mass spectrometric analysis were employed to confirm that analogues **1a**−**e**, FPP, and GPP were transferred by FTase to the *N*-dansyl-GCVLS peptide substrate. Samples for mass spectroscopy were obtained from 1 nmol scale

[2] $\{(i\text{-}PrO)_2POCH_2CO_2Et$, DBU, LiCl, CH_3CN, rt$\}$; (b) $\{(i\text{-}PrO)_2POCH_2CO_2Et$, DBU, LiCl, CH_3CN, reflux$\}$; (c) $\{(i\text{-}PrO)_2POCH_2CO_2Et$, NaH, DME, reflux$\}$ (*80*); (d) $\{(EtO)_2POCH_2CO_2Et$, DBU, LiCl, CH_3CN, rt$\}$; (e) $\{(EtO)_2POCH_2CO_2Et$, NaH, C_6H_6, 60 °C$\}$ (*71*); (f) $\{(EtO)_2POCH_2CO_2Et$, NaH, THF, rt$\}$ (*81*, *82*).

Table 1: HPLC Retention Time Comparison of Isoprenyl Pyrophosphate and *N*-Dansyl-GC(lipid)VLS Peptide

substrate	lipid length (atoms)[a]	lipid carbons	HPLC t_R[b] (min)	HPLC t_R, *N*-dansyl-GC(lipid)VLS (min)
GGPP	16	20	ND	ND
FPP	12	15	24.8	27.1
GPP	8	10	19.4	22.6
B2PP (**1a**)	11	13	18.6	21.9
B3PP (**1b**)	12	14	19.3	22.8
B4PP (**1c**)	13	15	20.6	23.8
B5PP (**1d**)	14	16	22.0	24.9
B6PP (**1e**)	15	17	22.9	25.9

[a] Assuming benzyl group is an isostere for an isoprene group. [b] Purified by analytical HPLC performed on a Waters HPLC controller and a Waters 2487 dual λ absorbance detector monitoring at 214 and 254 nm with a Western Analytical 250 × 4.6 mm, 5 μm BioBasic8 C_8 column. Compounds were eluted under the following gradient at a flow rate of 1 mL/min: 0−5 min, 100% A; 5−37 min, 10% A; 37−40 min, 10% A; 40−45 min, 100% A; 45−50 min, 100% A. Solvents: A = 25 mM NH_4HCO_3; B = CH_3CN. ND = not determined. HPLC t_R for *N*-dansyl-GCVLS = 13.4 min.

transfer reactions for each of the substrates. Reverse phase HPLC analysis of the reaction mixtures indicated quantitative conversion of the parent peptide to the *N*-dansyl-GC(lipid)-VLS peptide by the appearance of new peaks with retention times characteristic for alkylated pentapeptides (data not shown) (*32*−*35*). The new peaks in the HPLC chromatograms corresponding to the modified peptides were isolated, and lipid transfer was confirmed by high-resolution ESI mass spectrometry. The products of analogue transfer catalyzed by FTase to the peptide have increased hydrophobicity relative to the unmodified peptide. This is reflected in longer retention times compared to the parent peptide as shown in Table 1. The retention times of the peptides modified with analogues **1a**−**e** and the parent pyrophosphates increased monotonically with increasing chain length. As expected, there is a linear correlation between the retention times of the modified peptides and the parent pyrophosphates.

In these reactions, the *Z* α-isoprene isomer of the analogue pyrophosphates was present at approximately 11% of the total analogue pyrophosphate concentration. Remarkably, the *Z* α-isoprene isomer of FPP is a transferable substrate for FTase with a catalytic efficiency that is 41% of FPP (*16*). Therefore, we do not consider the effect of the minor *Z* α-isoprene isomers of the analogue pyrophosphates in our analysis of the FTase-catalyzed transfer reactions.

*Analogues **1a**−**e** and GPP Are Transferred with Lower Efficiency than FPP.* Steady-state kinetic parameters for transfer of FPP, GPP, and analogues **1a**−**e** for the transfer of lipid to the *N*-dansyl-GCVLS pentapeptide were measured and are reported in Table 2. Lipid pyrophosphates were incubated at various concentrations with FTase and 1.0 μM *N*-dansyl-GCVLS peptide, and initial reaction velocities were calculated from the time-dependent increase in fluorescence at each substrate concentration (Figure 2). These values were used to determine the kinetic parameters K_m, V_{max}, k_{cat}, and k_{cat}/K_m of FPP, GPP, and analogues **1a**−**e** (Table 2). The kinetic values obtained for FPP compared favorably to those reported in the literature (K_m = 40 nM, k_{cat} = 0.09 s^{-1}, k_{cat}/K_m = 2 × 10^6 M^{-1} s^{-1}) (*18*, *85*). While GPP and the BnPP class of analogues are alternative substrates for FTase-catalyzed transfer to the pentapeptide *N*-dansyl-GCVLS, all

Table 2: Steady-State Kinetic Parameters

substrate	K_m (nM)	k_{cat} (s^{-1} × 10^{-3})	k_{cat}/K_m (×10^5 M^{-1} s^{-1})	V_{rel}
GGPP	40[a]	–	–	–
FPP	46 ± 2	100 ± 3	22 ± 1	1.0
GPP	450 ± 30	15 ± 0.5	0.34 ± 0.03	0.015
B2PP (**1a**)	890 ± 50	44 ± 1	0.49 ± 0.03	0.022
B3PP (**1b**)	130 ± 5	8.4 ± 0.3	0.67 ± 0.03	0.030
B4PP (**1c**)	56 ± 3	27 ± 1	4.9 ± 0.3	0.22
B5PP (**1d**)	91 ± 5	43 ± 1	4.7 ± 0.3	0.21
B6PP (**1e**)	89 ± 5	25 ± 0.7	2.8 ± 0.2	0.13

[a] K_i value estimated from an IC_{50} value of 0.28 μM (*101*) for GGPP when a value for S = [GGPP] = 0.25 μM (*101*) is used (*18*). This value is in agreement with the finding that GGPP and FPP compete at essentially the same concentrations (*21*).

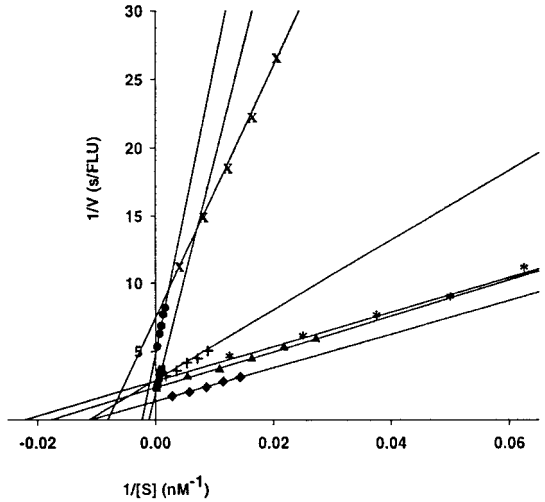

FIGURE 2: Lineweaver−Burk plots for FPP, GPP, and BnPP analogues. Each value is the average of quadruplicate incubations in the presence of the indicated concentration of GPP (●), FPP (*), B2PP (■), B3PP (×), B4PP (▲), B5PP (◆), or B6PP (+), and is representative of one experiment. Concentrations for each analogue were distributed around its K_m. FLU represents an arbitrary fluorescence unit.

of the analogues were poorer substrates than FPP. The most efficiently transferred analogue, **1c**, was transferred with a 5-fold lower velocity (k_{cat}/K_m) than FPP. Although geranylgeranyl pyrophosphate (GGPP) is not transferred by FTase to substrate peptide, FTase binds FPP and GGPP with similar affinities (*21*).

Analogue Hydrophobicity Correlates with 1/K_m. Analysis of the kinetic pathway indicates that FTase proceeds through a functionally ordered mechanism in which FPP binds first to the enzyme, with the overall equilibrium dissociation constant of FPP in the low nanomolar range (*86*, *87*). The protein substrate binds to the E·FPP complex in a fashion that is essentially irreversible (*87*, *88*). In addition to proteins, short peptides containing the appropriate Ca_1a_2X sequences can be used as efficient substrates by protein farnesyltransferases (*22*, *89*). For mammalian FTase, substrate binding and product release are rate-limiting for steady-state catalysis under conditions of subsaturating and saturating substrate concentrations, respectively (*87*, *90*). The K_M for FPP does not simply reflect the K_D for FPP when peptide concentration is saturating, assuming that FTase follows an ordered binding scheme (*91*). The K_M for FPP may reflect the binding of FPP to the E·product complex to accelerate product dissociation (*90*).

The K_m for analogues **1a**−**e** generally decreases with increasing chain length with a minimum for **1c** and rising again slightly for the longer **1d** and **1e** analogues (Table 2). Hydrophobicity is correlated with $1/K_m$ for FPP, GPP, and analogues **1a**−**e** ($R^2 = 0.7$). Analogue **1e** is three atoms longer than FPP and one atom shorter than GGPP in its all-trans conformation (Table 1). The K_m values for **1d** and **1e** level off even though **1e** is more hydrophobic, suggesting that K_m is also dependent on the lipid binding geometry. The correlation between hydrophobicity and $1/K_m$ is significantly improved by removing the data for **1e** ($R^2 = 0.86$). These results imply that the FTase·**1e** binding geometry may be less optimal for catalysis. While FPP and **1b** have the same length in their extended conformations, FPP is considerably more hydrophobic (Table 1). Based on HPLC retention times, **1b** has the same hydrophobicity as GPP although GPP has four fewer carbons. The lowered K_m for the BnPP analogues relative to FPP and GGPP is therefore likely to result from the ether oxygen and the increased conformational flexibility in the chain. It appears that the additional conformational freedom in the alkyl ether chain and desolvation of the ether oxygen upon FTase binding by the BnPP analogues carry a significant energetic cost. The differences in K_m most likely arise from the lipid−FTase interactions since molecular modeling of the binary complexes indicates that the electrostatic energy from pyrophosphate binding is similar for all of the analogues (see below).

k_{cat} Is Not Correlated with Analogue Hydrophobicity or Analogue Length. There is no simple relationship between k_{cat} and either the length or the hydrophobicity of the molecules examined in this study (Table 2). For FTase-catalyzed transfer of FPP to peptide substrate, k_{cat} is rate-limiting and corresponds to product release (*88*, *91*). The interactions between the alkylated peptide and FTase should be correlated with k_{cat} if it is not dependent on the chemical steps of the reaction and only on product release. The lack of a correlation between the hydrophobicity of the product peptide and k_{cat} coupled with the observation that k_{cat} for FPP is greater than that for GPP implies a significant kinetic contribution of the other steps in the mechanism for the transfer of GPP and the BnPP analogues. In addition, GGPP is more hydrophobic than FPP and is not transferred by FTase to peptide substrate. The rate of analogue transfer is high for **1a**, falls precipitously for **1b**, and then rises for **1c** and **1d** before falling again for **1e**. Interestingly, FPP and **1b** have the same fully extended length but have the highest and lowest k_{cat} values, respectively (Table 2). Structurally, **1b** lacks the β-isoprene double bond and branched methyl group. These results suggest that the variation in k_{cat} for the analogues may reflect differences in the binding geometry of the analogue and peptide substrate relative to FPP. This view is strengthened by the observation that while **1e** is only one carbon shorter than GGPP, it is transferred with a k_{cat} one-fourth that of FPP while GGPP is not transferred at all. Clearly, the interactions between the lipid pyrophosphate, peptide, and FTase that determine k_{cat} are dependent on the structure of the lipid.

FTase-Catalyzed Transfer of Lipid to N-Dansyl-GCVLS Is Dependent on Analogue Length. The efficiency of transfer (k_{cat}/K_m) for the BnPP analogues is maximum for **1c** and **1d**, which are one and two carbons longer than FPP in its fully extended conformation, respectively (Table 2). Interestingly, the chain length for maximum k_{cat} is found for analogues **1a** and **1d** while the minimum K_m is found for **1c**. Analogues **1c** and **1d** differ in length by one carbon, suggesting that there is a compromise between the conformation of the ternary complex best suited for catalysis and the optimal interaction of the lipid with the FTase·product complex to accelerate product dissociation. This idea is further supported by the observation that the k_{cat} for **1a** is 44% of that for FPP but that the K_m for **1a** is 19-fold greater than that for FPP. In addition, while GPP is three atoms shorter and has a K_m half that of analogue **1a**, it is transferred to substrate only 34% as fast as **1a**. Therefore, it is likely that the larger **1a** makes more productive contacts in the ternary complex than does the smaller GPP.

Interestingly, although **1c**, **1d**, and **1e** are all longer than FPP in their fully extended all-trans conformations, they are transferred to the target peptide while GGPP is not. FTase is a heterodimeric zinc metalloenzyme in which the metal ion plays a catalytic role (*21*, *92*−*94*). The zinc atom in FTase is located in the β subunit near the α/β subunit interface and marks the location of the active site (*23*). The β subunit is folded into an α/α barrel whose central cavity provides a deep hydrophobic cleft along one side to which the isoprenoid moiety of FPP binds (*24*). The C_1 position of the FPP molecule in the binary FPP·FTase X-ray crystal structures is in register with, but not bound to, the catalytic zinc ion (*23*). This observation suggests that the C_1 carbon of the lipid pyrophosphate must be in register with the zinc ion in order for efficient catalysis to occur. Binding of the shorter analogues may create a void in the pocket which interferes with productive binding by either the lipid or the peptide substrate. X-ray structural analysis has demonstrated that the peptide in the ternary complex is found in intimate contact with the farnesyl lipid (*25*, *26*). Additional stabilization of the ternary complex for productive transfer could result from van der Waals contacts between the a_2 and X residues of the peptide and the FPP that may be absent in the shorter GPP and **1a** substrates.

The inability of the BnPP series of molecules to be transferred with the same efficiency as FPP is likely due to differences in the structure of the linker arm. The BnPP linker chain is comprised of flexible methylene units, and has a larger number of conformations available to it compared with the more rigid FPP isoprenes. The three isoprenes of FPP may serve to preorganize the molecule to fit into the isoprenoid binding site of FTase, thereby reducing the number of conformations needed to place the pyrophosphate in register with the zinc atom and cysteine thiol of the peptide substrate. Because the BnPP class of molecules are less organized than FPP, once the molecule has bound in the FPP binding site, the lipid must find the optimal geometric fit. This may ultimately decrease the overall rate of the transfer reaction. Additionally, interactions between the farnesyl chain and the Ca_1a_2X peptide in the ternary complex are likely to be dependent on the specific shape of the lipid chain. In the case of the BnPP series, the lack of branched methyl groups may result in sub-optimal interactions in the ternary complex.

Modeling Provides a Molecular Explanation That an Aromatic Ring Is a Good Isostere for the Terminal Isoprene of FPP. An essential feature of FTase is its ability to discriminate against both GPP and GGPP in favor of FPP. Potential binding geometries of FPP, GPP, GGPP, and

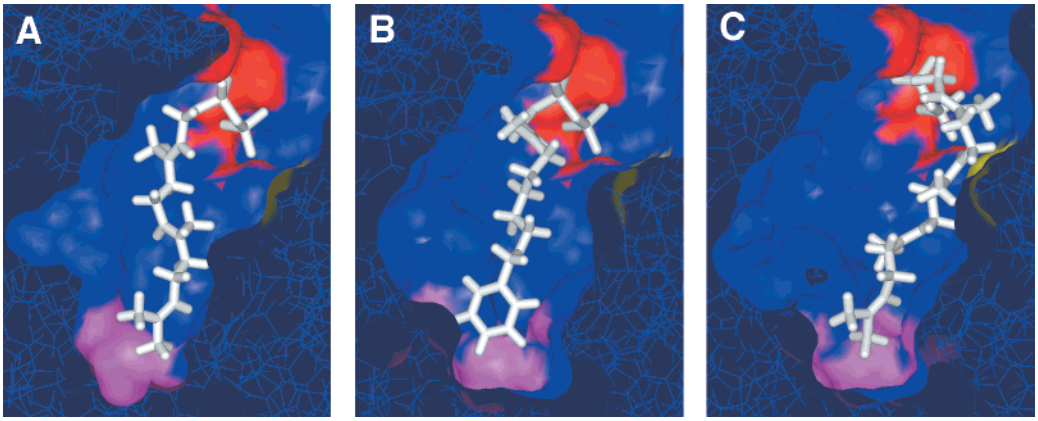

FIGURE 3: Cross section of FTase active site surface with pyrophosphate coordinating region in red, terminal isoprene "slot" in magenta, catalytic zinc in yellow, and stick rendering of isoprenoid or BnPP in white. (A) FPP from minimized modified 1FT2 crystal structure, (B) modeled B4PP showing terminal benzene inserted into slot, and (C) modeled GGPP showing proper coordination of pyrophosphate and insertion of terminal isoprene into slot, but occlusion of peptide binding region that precludes efficient transfer. Cross sections are slightly different from one another in order to best display the binding of each ligand. Active site residues that were allowed to move during modeling superimpose with an RMSD of 0.30 Å between (A) and (B), which is similar to the RMSD of 0.27 Å for these residues between binary cocrystal structures 1FT2 and 1FPP.

analogues **1a**−**e** were examined by modeling the molecules into the active site of the FTase crystal structure. The procedure used to model the lipid pyrophosphates into the FTase active site reproduced the conformation and geometry of FPP found in the binary X-ray crystal structures (*24*, *25*). Pairwise comparison of the position of the active site side chains between the two available FTase·FPP X-ray crystal structures and the calculated FTase·FPP model shows a 0.27 Å rms deviation, indicating that the model is accurate on the order of the variation in the independent X-ray crystal structure determinations. Examination of the FTase·FPP X-ray crystal structure and the individual contributions to the binding energy of the molecules calculated from the molecular models reveals several features that are important for substrate recognition.

Electrostatic interactions between the pyrophosphate of FPP and residues Lys 164β, His 248β, Arg 291β, Lys 294β, and Tyr 300β are calculated to be the dominant source of binding energy in the binary FTase·FPP complex. These electrostatic interactions fix the position of the pyrophosphate with respect to the catalytic zinc ion. These electrostatic interactions were also calculated to be the dominant source of binding energy for the FTase models with GPP, GGPP, and analogues **1a**−**e**. In addition to Zn^{2+}, Mg^{2+} is required for the catalytic mechanism and appears to coordinate the pyrophosphate moiety of FPP. However, removal of the Mg^{2+} ion does not affect substrate binding (*21*, *88*). The location of the magnesium ion is not defined in any of the X-ray crystal structures, and, therefore, the magnesium was not modeled into the complex. In addition, the electrostatic term for the binding energy of the lipid to FTase was still dominant when the charge on the pyrophosphate was reduced from −3 to −1.

Examination of the binary X-ray crystal structure shows that the terminal isoprene methyl groups of FPP fill a slot defined by side chains from Trp 102β, Tyr 205β, Phe 253β, Cys 254β, Trp 303β, and the aliphatic stretch of Arg 202β at the bottom of the active site (Figure 3A) (*24*, *25*). This "slot" at the floor of the active site is also visible in the X-ray crystal structure of FTase alone (*23*). Between the slot and the pyrophosphate binding site, the FPP chain is fully extended and bound against the side of the active site opposite that where the incoming peptide or protein C-terminus binds. Except for analogue **1a**, models of the complexes with the analogues have the terminal edge of the benzyl group occupying the slot at the floor of the FTase active site (Figure 3B). Analogue **1a** is too short for the benzyl group to bind into the slot when its phosphate is in register with the zinc ion. Similarly, the model of GPP bound to FTase also shows that the terminal isoprene of GPP is unable to contact the residues within the slot. The loss of these van der Waals interactions and the subsequent void in the complex may contribute to the higher K_m and lower rate of catalysis for **1a** and GPP. The modeling suggests that the benzyl ring of analogue **1b** does not completely occupy the slot, while it is efficiently filled by the benzyl groups of **1c**−**e** (Figure 3B). The modeling results provide a molecular explanation for the observation that an aromatic ring is a good isostere for the terminal isoprene of FPP. The location of the volume occupied by the alkyl-ether chains of analogues **1a**−**e** in these models is coincident with that of the farnesyl chain in the binary complex. However, only analogue **1d** displaces approximately the same volume of the active site as does FPP, where analogues **1a**−**c** occupy lesser volumes and **1e** occupies a slightly larger volume.

The FTase Molecular Ruler for Isoprenoid Substrate Discrimination Is Dependent on Isoprene Double Bonds and Branched Methyl Groups. In agreement with the modeling results for GPP, FPP, and analogues **1a**−**e**, the pyrophosphate of GGPP was found in register with the zinc ion, and the terminal isoprene methyl groups were inserted into the slot at the floor of the active site (Figure 3C). However, in sharp contrast to the other molecules examined, the longer geranylgeranyl chain adopts a different conformation than the farnesyl chain of FPP, partially occluding the space occupied by the Ca_1a_2X peptide in the ternary X-ray crystal structure. Within the confines of the FTase pocket, the double bonds and branched methyl groups of the geranylgeranyl chain significantly restrict the number of possible conformations relative to analogues **1a**−**e**. Therefore, substrate discrimination by FTase may be achieved by the conformational restrictions that force the geranylgeranyl chain to traverse

the peptide binding site rather than conform to the farnesyl binding site. This model for FTase substrate discrimination contrasts with the previously proposed mechanism for substrate discrimination where transfer of the geranylgeranyl lipid to peptide is prevented because the C_1 position of GGPP is forced to protrude beyond the catalytic zinc ion (*23*, *24*).

Therefore, FTase might discriminate against transfer of GPP and GGPP in favor of FPP by two different mechanisms. The discrimination against the shorter GPP is apparently due to the lack of important interactions in the binary and/or ternary complex mediated by the terminal isoprene unit of FPP, while discrimination against the longer GGPP appears to stem from steric occlusion of the active site caused by the conformational rigidity of the geranylgeranyl chain.

Implications of Analogue Structures for Altering Downstream Ras Processing. While farnesylation is absolutely required for Ras function, it is unknown whether the prenyl group functions as a hydrophobic membrane association signal (*6*, *15*, *95*−*98*), a targeted farnesyl-protein recognition (*99*, *100*), or both. In contrast to FTIs, transferable FPP analogues allow the examination and study of the prenyl structure on downstream processing events. Previous studies have suggested that the hydrophobicity of the lipid, and not the precise structure, plays a prominent role in promoting the biological activity of H-Ras (*15*). Of particular interest will be studies to examine the biological function of transferable analogues where heteroatoms are introduced into the lipid chain to determine if hydrophobicity is indeed the primary determinant of H-Ras biological activity.

ACKNOWLEDGMENT

We thank Dr. Robert Dickson and Dr. Robert Lester for assistance with the HPLC fluorescence analysis, Dr. Louis Hersh for advice with the enzyme kinetics, and Dr. Carol Fierke and Jennifer Pickett for the gift of protein farnesyltransferase and careful reading of the manuscript.

SUPPORTING INFORMATION AVAILABLE

^{1}H, ^{13}C, ^{31}P NMR, and MS spectra for compounds **1a**−**e**; ^{1}H and ^{13}C NMR spectra for compounds **3a**−**e**; ^{1}H and ^{13}C NMR spectra for compounds **4a**−**e**; ^{1}H and ^{13}C NMR spectra for compounds **5a**−**e**; ^{1}H and ^{13}C NMR spectra for compounds **6a**−**c**; ^{1}H, ^{13}C NMR, and MS spectra for compounds **6d** and **6e**; ^{1}H and ^{13}C NMR spectra for compounds **7a** and **7b**; ^{1}H, ^{13}C NMR, and MS spectra for compounds **7c**−**e**; ^{1}H and ^{13}C NMR spectra for compound **8a**; ^{1}H, ^{13}C NMR, and MS spectra for compounds **8b**−**e**; MS spectra for compounds **9**, **10**, and **11a**−**e** (103 pages). This material is available free of charge via the Internet at http://pubs.acs.org.

REFERENCES

1. Zhang, F. L., and Casey, P. J. (1996) *Annu. Rev. Biochem. 65*, 241−269.
2. Hightower, K. E., and Fierke, C. A. (1998) *Curr. Opin. Chem. Biol. 3*, 176.
3. Sinensky, M. (2000) *Biochim. Biophys. Acta 1484*, 93.
4. Glomset, J. A., and Farnsworth, C. C. (1994) *Annu. Rev. Cell Biol. 10*, 181−205.
5. Parish, C. A., and Rando, R. R. (1996) *Biochemistry 35*, 8473−8477.
6. Hancock, J. F., Magee, A. I., Childs, J. E., and Marshall, C. J. (1989) *Cell 57*, 1167−1177.
7. Schafer, W. R., and Rine, J. (1992) *Annu. Rev. Genet. 30*, 209−237.
8. Gibbs, J. B., and Oliff, A. (1997) *Annu. Rev. Pharmacol. Toxicol. 37*, 143−166.
9. Leonard, D. M. (1997) *J. Med. Chem. 40*, 2971−2990.
10. Sebti, S. M., and Hamilton, A. D. (1997) *Pharmacol. Ther. 74*, 103−114.
11. Rowinsky, E. K., Windle, J. J., and Von Hoff, D. D. (1999) *J. Clin. Oncol. 17*, 3631−3652.
12. Sebti, S. M., and Hamilton, A. D. (2000) *Exp. Opin. Invest. Drugs 9*, 2767−2782.
13. Gibbs, R. A., Krishnan, U., Dolence, J. M., and Poulter, C. D. (1995) *J. Org. Chem. 60*, 7821.
14. Mu, Y. Q., Gibbs, R. A., Eubanks, L. M., and Poulter, C. D. (1996) *J. Org. Chem. 61*, 8010.
15. Dudler, T., and Gelb, M. H. (1997) *Biochemistry 36*, 12434−12441.
16. Shao, Y., Eummer, J. T., and Gibbs, R. A. (1999) *Org. Lett. 1*, 627−630.
17. Gibbs, B. S., Zahn, T. J., Mu, Y. Q., Sebolt-Leopold, J. S., and Gibbs, R. A. (1999) *J. Med. Chem. 42*, 3800.
18. Chehade, K. A. H., Andres, D. A., Morimoto, H., and Spielmann, H. P. (2000) *J. Org. Chem. 65*, 3027−3033.
19. Dolence, J. M., and Poulter, C. D. (1995) *Proc. Natl. Acad. Sci. U.S.A. 92*, 5008−5011.
20. Dolence, J. M., Cassidy, P. B., Mathis, J. R., and Poulter, C. D. (1995) *Biochemistry 34*, 16687−16694.
21. Reiss, Y., Brown, M. S., and Goldstein, J. L. (1992) *J. Biol. Chem 267*, 6403−6408.
22. Reiss, Y., Goldstein, J. L., Seabra, M. C., Casey, P. J., and Brown, M. S. (1990) *Cell 62*, 81−88.
23. Park, H.-W., Boduluri, S. R., Moomaw, J. F., Casey, P. J., and Beese, L. S. (1997) *Science 275*, 1800−1804.
24. Long, S. B., Casey, P. J., and Beese, L. S. (1998) *Biochemistry 37*, 9612−9618.
25. Strickland, C. L., Windsor, W. T., Syto, R., Wang, L., Bond, R., Wu, Z., Schwartz, J., Le, H. V., Beese, L. S., and Weber, P. C. (1998) *Biochemistry 37*, 16601.
26. Long, S. B., Casey, P. J., and Beese, L. S. (2000) *Structure 8*, 209.
27. Baba, T., and Allen, C. M. (1984) *Biochemistry 23*, 1312−1322.
28. Baba, T., Muth, J., and Allen, C. M. (1985) *J. Biol. Chem. 260*, 10467−10473.
29. Allen, C. M. (1985) *Methods Enzymol. 110*, 117−124.
30. Bukhtiyarov, Y. E., Omer, C. A., and Allen, C. M. (1995) *J. Biol. Chem. 270*, 19035−19040.
31. Das, N. P., and Allen, C. M. (1991) *Biochem. Biophys. Res. Commun. 181*, 729−735.
32. Gaon, I., Turek, T. C., Weller, V. A., Edelstein, R. L., Singh, S. K., and Distefano, M. D. (1996) *J. Org. Chem. 61*, 7738−7745.
33. Gaon, I., Turek, T. C., and Distefano, M. D. (1996) *Tetrahedron Lett. 37*, 8833−8836.
34. Turek, T. C., Gaon, I., and Distefano, M. D. (1996) *Tetrahedron Lett. 37*, 4845−4848.
35. Edelstein, R. L., and Distefano, M. D. (1997) *Biochem. Biophys. Res. Commun. 235*, 377−382.
36. Turek, T. C., Gaon, I., and Distefano, M. D. (2001) *J. Org. Chem. 66*, 3253−3264.
37. Butler, C. L., Renfrew, A. G., and Clapp, M. (1938) *J. Am. Chem. Soc. 60*, 1472.
38. Mori, K., and Qian, Z. H. (1994) *Liebigs Ann. Chem. 3*, 291.
39. Quici, S., Manfredi, A., Raimondi, L., and Sironi, A. (1995) *J. Org. Chem. 60*, 6379.
40. Wasserman, D., and Dawson, C. R. (1942) *J. Org. Chem. 8*, 73.
41. Collins, P. M., and Eder, H. (1984) *J. Chem. Soc., Perkin Trans. 1 7*, 1525.
42. Hamilton, L., Stevenson, M. H., Boyd, D. R., Brannigan, I. N., Treacy, A. B., Hamilton, J. T. G., McRoberts, W. C., and Elliot, C. T. (1996) *J. Chem. Soc., Perkin Trans. 1 2*, 139.
43. Gowravaram, M. R., Tomczuk, B. E., Johnson, J. S., Delecki, D., Cook, E. R., Ghose, A. K., Mathiowetz, A. M., Spurlino,

J. C., Rubin, B., Smith, D. J., Pulvino, T., and Wahl, R. C. (1995) *J. Med. Chem. 38*, 2570.
44. Ginsburg, D., and Pappo, R. (1952) *J. Chem. Soc.*, 1524.
45. Lunney, E. A., Hagen, S. E., Domagala, J. M., Humblet, C., Kosinski, J., Tait, B. D., Warnus, J. S., Wilson, M., Ferguson, D., Hupe, D., Tummino, P. J., Baldwin, E. T., Bhat, T. N., Liu, B., and Erickson, J. W. (1994) *J. Med. Chem. 37*, 2664.
46. Scribner, A. W., Haroutounian, S. A., Carlson, K. E., and Katzenellenbogen, J. A. (1997) *J. Org. Chem. 62*, 1043.
47. Farr, R. A., Bey, P., Sunkara, P. S., and Lippert, B. J. (1989) *J. Med. Chem. 32*, 1879.
48. Howson, W., Taylor, E. M., Parson, M. E., Novelli, R., Wilczynska, M. A., and Harris, D. J. (1988) *Eur. J. Med. Chem. 23*, 433.
49. Tokoroiama, T., and Kusaka, H. (1996) *Can. J. Chem. 74*, 2487.
50. Morimoto, Y., and Yokoe, C. (1997) *Tetrahedron Lett. 38*, 8981.
51. Morimoto, Y., Yokoe, C., Kurihara, H., and Kinoshita, T. (1998) *Tetrahedron 54*, 12197.
52. Ducray, P., Lebeau, L., and Mioskowski, C. (1996) *Helv. Chim. Acta 79*, 2346.
53. Cossy, J., Ranaivosata, J. L., Bellosta, V., and Wietzke, R. (1995) *Synth. Commun. 25*, 3109.
54. Mahboobi, S., and Bernauer, K. (1988) *Helv. Chim. Acta 71*, 2034.
55. Tipson, R. S., Clapp, M. A., and Cretcher, L. H. (1947) *J. Org. Chem. 12*, 133.
56. Ludeman, S. M., Bartlett, D. L., and Zon, G. (1979) *J. Org. Chem. 44*, 1163.
57. Macdonald Bennet, G., and Hock, A. L. (1927) *J. Chem. Soc.*, 472.
58. Liu, C., and Coward, J. K. (1991) *J. Med. Chem. 34*, 2094.
59. Berlage, U., Schmidt, J., Peters, U., and Welzel, P. (1987) *Tetrahedron Lett. 28*, 3091.
60. Cohen, N., Banner, B. L., Blount, J. F., Weber, G., Tsai, M., and Sancy, G. (1974) *J. Org. Chem. 39*, 1824.
61. Paulvannan, K., Schwartz, J. B., and Stille, J. R. (1993) *Tetrahedron Lett. 34*, 215.
62. Singerman, G. M., Kimura, R., Riebsomer, J. L., and Castle, R. N. (1966) *J. Heterocycl. Chem. 3*, 74.
63. Soai, K., and Watanabe, M. (1991) *Tetrahedron Asymm. 2*, 97.
64. Kuroda, C., and Ito, K. (1996) *Bull. Chem. Soc. Jpn. 69*, 2297.
65. Cannon, J. R., and Metcalf, B. W. (1973) *Aust. J. Chem. 26*, 2277.
66. Watanabe, M., and Soai, K. (1994) *J. Chem. Soc., Perkin Trans. 1 7*, 837.
67. Sargent, M. V., and Wangchareontrakul, S. (1990) *J. Chem. Soc., Perkin Trans. 1 1*, 129.
68. Battersby, A. R., Howson, W., and Hamilton, A. D. (1982) *J. Chem. Soc., Chem. Commun. 2*, 1266.
69. Jiang, J. B., Urbansky, M. J., and Hajos, Z. G. (1983) *J. Org. Chem. 48*, 2001.
70. Bosseray, P., Guillaumet, G., Coudert, G., and Wassermann, H. (1989) *Tetrahedron Lett. 30*, 1387.
71. Gurjar, M. K., and Saha, U. K. (1993) *Tetrahedron Lett. 34*, 1833.
72. Hoffmann, M. G., and Schmidt, R. R. (1985) *Liebigs Ann. Chem. 12*, 2403.
73. Hasserodt, J., Janda, K. D., and Lerner, R. A. (1997) *J. Am. Chem. Soc. 119*, 5993.
74. Mitra, R. B., and Bhaskar Reddy, G. (1989) *Synthesis 9*, 694.
75. Pompliano, D. L., Gomez, R. P., and Anthony, N. J. (1992) *J. Am. Chem. Soc. 114*, 7945−7946.
76. Cassidy, P. B., Dolence, J. M., and Poulter, C. D. (1995) *Methods Enzymol. 250*, 30−43.
77. Zimmerman, K. K., Scholten, J. D., Huang, C.-C., Fierke, C. A., and Hupe, D. J. (1998) *Protein Expression Purif. 14*, 395−402.
78. Pang, Y.-P., Xu, K., El Yazal, J., and Prendergast, F. G. (2000) *Protein Sci. 9*, 1857−1865.
79. Cieplak, P., Cornell, W. D., Bayly, C., and Kollman, P. A. (1995) *J. Comput. Chem. 16*, 1357−1377.
80. Klinge, S., and Demuth, M. (1993) *Synlett*, 783.
81. Chiarello, J., and Joullie, M. M. (1988) *Tetrahedron 44*, 41−48.
82. Gao, W.-G., Sakaguchi, K., Isoe, S., and Ohfune, Y. (1996) *Tetrahedron Lett. 37*, 7071−7074.
83. Davisson, V. J., Woodside, A. B., and Poulter, C. D. (1985) *Methods Enzymol. 110*, 130−144.
84. Davisson, V. J., Woodside, A. B., Neal, T. R., Stremler, K. E., Muehlbacher, M., and Poulter, C. D. (1986) *J. Org. Chem. 51*, 4768−4779.
85. Pompliano, D. L., Rands, E., Schaber, M. D., Mosser, S. D., Anthony, N. J., and Gibbs, J. B. (1992) *Biochemistry 31*, 3800−3807.
86. Pompliano, D. L., Schaber, M. D., Mosser, S. D., Omer, C. A., Shafer, J. A., and Gibbs, J. B. (1993) *Biochemistry 32*, 8341−8347.
87. Furfine, E. S., Leban, J. J., Landavazo, A., Moomaw, J. F., and Casey, P. J. (1995) *Biochemistry 34*, 6857−6862.
88. Huang, C.-C., Hightower, K. E., and Fierke, C. A. (2000) *Biochemistry 39*, 2593.
89. Yokoyama, K., Goodwin, G. W., Ghomashchi, F., Glomset, J. A., and Gelb, M. H. (1991) *Proc. Natl. Acad. Sci. U.S.A. 88*, 5302−5306.
90. Tschantz, W. R., Furfine, E. S., and Casey, P. J. (1997) *J. Biol. Chem. 272*, 9989−9993.
91. Saderholm, M. J., Hightower, K. E., and Fierke, C. A. (2000) *Biochemistry 40*, 12398−12405.
92. Chen, W.-J., Moomaw, J. F., Overton, L., Kost, T. A., and Casey, P. J. (1993) *J. Biol. Chem. 268*, 9675−9680.
93. Moomaw, J. F., and Casey, P. J. (1992) *J. Biol. Chem. 267*, 17438−17443.
94. Huang, C.-C., Casey, P. J., and Fierke, C. A. (1997) *J. Biol. Chem. 272*, 20−23.
95. Hancock, J. F., Cadwallader, K., Paterson, H., and Marshall, C. J. (1991) *EMBO J. 10*, 4033−4039.
96. Hancock, J. F., Cadwallader, K., and Marshall, C. J. (1991) *EMBO J. 10*, 641−646.
97. Leevers, S. J., Paterson, H. F., and Marshall, C. J. (1994) *Nature 369*, 411−414.
98. Stokoe, D., Macdonald, S. G., Cadwallader, K., Symons, M., and Hancock, J. F. (1994) *Science 264*, 1463−1467.
99. Marshall, C. J. (1993) *Science 259*, 1865−1866.
100. Casey, P. J. (1995) *Science 268*, 221−225.
101. Moores, S. L., Schaber, M. D., Mosser, S. D., Rands, E., O'Hara, M. B., Garsky, V. M., Marshall, M. S., Pompliano, D. L., and Gibbs, J. B. (1991) *J. Biol. Chem. 266*, 14603−14610.

BI011133F